Reports

Oblique Impact: A Process for Obtaining Meteorite Samples from Other Planets

John D. O'Keefe and Thomas J. Ahrens

Cratering flow calculations for a series of oblique to normal (10° to 90°) impacts of silicate projectiles onto a silicate halfspace were carried out to determine whether or not the gas produced upon shock-vaporizing both projectile and target material would form a downstream jet that could entrain and propel SNC meteorites from the Martian surface. The difficult constraints that the impact origin hypothesis for SNC meteorites has to satisfy are that these meteorites are lightly to moderately shocked and yet have been accelerated to speeds in excess of the Martian escape velocity (more than 5 kilometers per second). Two-dimensional finite difference calculations were performed that show that at highly probable impact velocities (7.5 kilometers per second), vapor plume jets are produced at oblique impact angles of 25° to 60° and have speeds as great as 20 kilometers per second. These plumes flow nearly parallel to the planetary surface. It is shown that upon impact of projectiles having radii of 0.1 to 1 kilometer, the resulting vapor jets have densities of 0.1 to 1 gram per cubic centimeter. These jets can entrain Martian surface rocks and accelerate them to velocities greater than 5 kilometers per second. This mechanism may launch SNC meteorites to earth.

All meteorites—stones, irons, primitives, and differentiates—are samples of other larger objects in the solar systems in that they exhibit features of planetary processes varying from slight aqueous metamorphism (*1*), crystallization under different cooling histories (*2*), or crystallization in a substantial gravity field (*3*). Some classes of stony meteorites, the shergottites (S), nakhlites (N), and Chassigny (C) (collectively, called SNC meteorites) (*4*), are unique in present terrestrial collections. These stones are a small fraction (eight) out of the total number of meteorites (10^4). The SNC meteorites, which as early as 1979 were proposed by Wasson and Wetherill (*5*) to be samples of Mars, appeared to be so for a number of reasons.

1) They have distinct crystallization ages of 1.3×10^9 years, whereas all other meteorites (*6*) have a crystallization age of 4.6×10^9 years (*7*). Some discrepancies in ages are demonstrated by the more heavily shocked shergottites (*4*).

2) The SNC meteorites show a distinctive $\delta^{17}O$–$\delta^{18}O$ fractionation trend which is displaced from all other samples of the earth, the moon, and other meteorites, including the petrologically similar basaltic achondrites (eucrites) (*8*).

3) The shergottites are heavily shocked basalts with high volatile element abundances consistent with the Martian soil analyses (*9*). The lightly, or unshocked, nakhlites (clinopyroxenites) and Chassigny (dunite) appear to be more deep seated gravity cumulate rocks that appear, like many earth rocks, to have been slightly oxidized. Other evidence of formation on a planet with a strong gravity field comes from the general high degree of rare earth enrichment and the lack of a europium anomaly (*10*).

4) Both the relative abundance and isotopic composition of the argon, krypton, xenon, and nitrogen in the glass of the heavily shocked shergottites are different from those found in other meteorites, the earth, or Venus (*11*). Their composition is close to that of the Martian atmosphere as measured by Viking, suggesting that it was emplaced during an impact event on Mars in the Martian atmosphere. The Rb-Sr date of 180 million years (m.y.) in the shergottites may record such an impact event.

Cosmic ray exposure ages of 0.4 to 12 m.y. (*4*) for SNC meteorites place important constraints on the size and transit time to the earth. If the impact age (180 m.y.) corresponds to the time of ejection, then the low level of cosmic ray exposure can only be explained by the meteorite sample having been imbedded within an object having a diameter of about 10 m. Conversely, if the 180 m.y. event did not launch ejecta to velocities exceeding the Martian escape velocity, then 10-cm sized objects are consistent with transit times on the order of the cosmic ray exposure age (*12*).

One of the key issues associated with the origin of SNC meteorites is how, if they are samples of a planet with substantial gravity, are they ejected from the planet and yet satisfy the above constraints? This issue is more critical for "Martian" meteorites than meteorites of "lunar" origin (*13*) on account of the substantially lower escape velocity of the moon. The entrainment of gases in the shock-induced melt within some of the shergottites with exactly the same number density per unit volume as in the Martian atmosphere as observed by the Viking landers (*14*) suggests that the samples were ejected from the planet by some aspect of the impact process. Several ejection mechanisms have been proposed. These include (i) normal impact ejection, (ii) spallation, (iii) impact vapor drag acceleration, and (iv) shallow angle impact ejecta acceleration. None of the above mechanisms satisfies all of the constraints, or is supported by detailed analysis and experiments, or both.

Ejection of material by near normal angle (>80°) impacts is difficult because the planetary material is accelerated by a shock process. Simple shock state calculations as well as detailed impact flow field calculations show that silicate ejecta that has velocities exceeding the Martian escape velocity (>5 km/sec) will be molten or partially vaporized (*15*). This conclusion is incompatible with the non- or lightly shocked condition of the nakhlites and Chassigny and only marginally agrees with the moderate shock history of the shergottites.

Melosh (*13*) proposed that the reflection of the impact shock wave from the planetary surface would result in spallation of the surface and ejection of lightly shocked high speed fragments. His calculations imply that centimeter-sized fragments could escape from the moon but probably not from Mars. One of the difficulties with this mechanism is that spallation fragments at high velocities have not been observed in impact experiments (*16*), although these were at a smaller scale than planetary events.

Acceleration of impact ejecta and surface rocks by impact induced vapor has been proposed as a mechanism for producing high speed objects (*17–20*). Singer (*18*) modeled a normal impact produced vapor plume as an expanding hemispherical cloud in which crater fragments were ejected and concluded that rocks greater than 1 m in diameter could not be accelerated to Martian escape velocities. Note that detailed numerical code calculations of normal high velocity impacts with substantial vaporization give vapor cloud plumes that are directed away from the surface and do not effectively entrain crater ejecta (*15*). Nyquist (*19*) proposed that a vapor cloud produced by a shallow angle impact (<10°) would acceler-

Seismological Laboratory 252-21, California Institute of Technology, Pasadena, CA 91125.

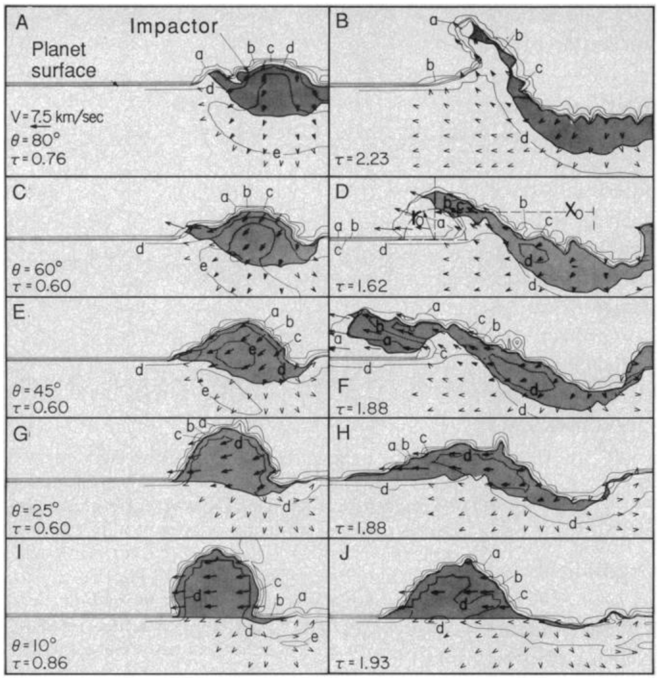

Fig. 1. Particle velocity and density flow fields for 2.7 g/cm^3 silicate projectile hitting a silicate planet at 7.5 km/sec at oblique angles of 80° (A and B); 60° (C and D); 45° (E and F); 25° (G and H); and 10° (I and J). Density contours: a, 0.1; b, 0.5; c, 1.0; d, 2.7; and e, 3.5 g/cm^3. Nondimensional time, τ, is real time times impact velocity divided by projectile diameter.

ate rocks to Martian escape velocities. The calculations presented here and experiments (*21*) show that significant vaporization does not occur in shallow angle impacts.

Nyquist (*19*) suggested that multiple impacts of crater ejecta on surface rocks could accelerate them to Martian escape velocity without heavily shocking them. This mechanism is not consistent with the oblique impact calculations discussed below. Although Zook *et al.* and Gault and Wedekind (*22*) have shown enhanced ejecta production for impacts at oblique angles, they did not demonstrate the combined constraints of Mars' origin: high velocity and minimal shock metamorphism that appear to be required.

We calculated the flow fields for normal and oblique impacts using a two-dimensional numerical computational algorithm (*23*). The algorithm accurately models the flow field for normal impacts since in that case the flow has axial symmetry. In the case of oblique impacts, the two-dimensional model is an approximation to the three-dimensional flow field and is only accurate in the plane described by the angle of impact. Thus we actually describe the oblique impact of a cylinder on a semi-infinite halfspace. The equation of state that we employed was generic of silicates as they might exist on Mars. We assume a density and bulk modulus of 2.7 g/cm^3 and 800 kbar for both the projectile and target. This would correspond to 92% enstatite, mass fraction, and 8% water. The enthalpy of incipient vaporization is 3.3 kJ/g from STP or 0.85 of that of pure enstatite. The enthalpy of vaporization was taken to be about 12 kJ/g and was varied from 0.12 kJ/g to 18 kJ/g to model effects of varying the volatility. The strength properties of the rock were neglected as those are unimportant in the modeling of high speed ejecta (>1 km/sec) (*24*).

Flow fields were calculated for impact angles ranging from 90° (normal impact), 80°, 60°, 45°, 25°, 10°, and velocities characteristic of low speed (7.5 km/sec) and high speed (20 km/sec) events. The low speed is close to the mean value for impactors on Mars, which is 8 to 12 km/sec (*25*).

The resulting density and particle velocity flow fields for an impact velocity of 7.5 km/sec are shown in Fig. 1. The vectors indicate the magnitude and direction of the velocity field and the contours delineate the density distribution. The nature of the flow field changes with impact angle and can be described in terms of three regimes: circular cratering, jetting, and skimming.

In the circular cratering regime nearly circular, relatively deep craters are produced and the flow fields are initiated by a single shock process. This regime occurs for impact angles ranging from 90° to at least 80°. The fastest moving downstream ejecta velocity and angle of the ejection does not vary significantly with time. The ejecta are propelled at angles about 45° relative to the planetary surface, and this angle decreases to about 10° as the impact angle decreases to 45°. For impact velocities of 7.5 km/sec the initial high speed ejecta is highly shocked and melted but not vaporized; for impact velocities of 20 km/sec, the high speed ejecta is vaporized.

In the jetting regime, impact angle (60° to 25°), the crater is shallower and can exhibit complex configurations as has been shown in experiments (*26*). The ejecta velocity is approximately constant until jetting starts to occur at impact angles of approximately 60°. The maximum downstream ejecta velocity increases significantly with decreasing impact angle and reaches a maximum of nearly 20 km/sec at oblique angles of 25° for impacts of 7.5 km/sec (Fig. 2). The ejecta angle decreases rapidly with impact angle and much of the flow is within 5° of the surface for impact angles less than 60° (Fig. 2). The density contours show that the jet flowing across the surface is primarily low density vaporized planetary and impactor material. Qualitatively this flow is similar to those recently observed photographically by Schultz and Gault (*21*) upon oblique impact onto CO_2-bearing targets in the laboratory. The amount of mass vaporized is about 0.3 the mass of the impactor for the 7.5 km/sec and 45° case. The amounts of Martian surface material that can be accelerated to more than 5 km/sec will then be a fraction of this gas mass. The flow field in this regime is not solely initiated by a single shock process; multiple shock processes occur in the downstream direction and give rise to vaporization and jetting even at the relatively low impact velocity of 7.5 km/sec. The rapid increase in the downstream ejecta velocity to more than twice the impact velocity is a consequence of this jetting. The conditions for jetting are not satisfied for impact angles less than 15° (*27*). The downstream high speed ejecta consists of both planetary and impactor material for impact angles greater than 25° for low speed impactors.

The effect of varying the volatility of the planetary surface on the vapor plume was also examined. The vaporization energy was increased by a factor of 1.5 to simulate a refractory planetary surface (for example, the moon) and decreased by an order of magnitude to simulate an extremely volatile-rich surface (for example, Mars' polar regions). At an impact velocity of 7.5 km/sec and angle of 45°, volatility did not have a large effect on the jet plume characteristics. The plume velocity increased by 15% and the plume mass was within 10% of the nominal value for a decrease in vaporization energy of an order of magnitude. In the low vaporization energy case, the plume cloud was larger at a given time as compared to the nominal case; however, the density was lower. The reason for this is that the multiple shock region that creates the jet plume is localized, and thus it restricts the amount of material that can be vaporized; in addition, the temperatures in that region are well above that required to vaporize even very refractory rocks. A greater difference would be expected at lower but less probable impact velocities, where the shock region is at the threshold for vaporization.

At impact angles less than 25°, the skimming regime occurs and the projectile is eroded as it skids along the planetary surface. No substantial penetration of the planetary surface occurs. In this case only the impactor material constitutes the small ejecta jet.

Examining the flow fields in Fig. 1 suggests that the high velocity vapor plumes that are produced by oblique impacts could be a mechanism for accelerating surface rocks to velocities in excess of Martian escape velocity. We outline a simple model for determining the conditions for accelerating surface rocks under lightly shocked and unfractured conditions.

The present calculations are a good approximation to the flow field in the plane of incidence and close to the point of impact. We developed a model for the flow field in the plane of incidence that approximately accounts for the out of plane expansion of the vapor at points downstream from the point of impact.

The finite extent and duration of the cloud arises from the jet source, which is the multiple shock interaction region. The nonstationary vapor source propagates along the surface, and provides vapor having a high expansion velocity.

For impact velocities of 7.5 km/sec and impact angles ranging from 45° to 60°, the vapor plume was modeled as an expanding hemi-torus in the downstream direction.

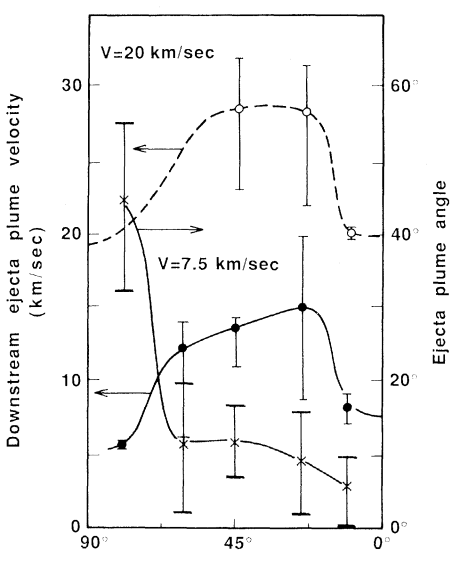

Fig. 2. Downstream ejecta-gaseous plume velocity as a function of impact angle for 7.5- and 20-km/sec silicate projectile hitting a silicate planet (left). All flows calculated are similar to those in Fig. 1. Range of angles between downstream ejecta plume flow direction and planetary surface for 7.5 km/sec impact is shown on the right. Bars represent range of values observed in calculated flow fields.

With this assumption, the vapor plume density as a function of distance along the surface is given by

$$\rho_g = \rho_{g0}\left(\frac{x_0}{x}\right)\left(\frac{r_0}{r(x)}\right)^2 \qquad (1)$$

where ρ_{g0} is the mean computed density of the jet plume at a mean position x_0 and r_0 is the mean radius of the semicircle (see Fig. 1D). The (x/x_0) term accounts for the decrease in density from expansion of the gas perpendicular to the plane of impact; the (r_0/r) term accounts for the radial expansion of the vapor plume in the plane of impact. Here r and x are the minor and major radii of the hemi-torus. The radius of the plume as a function of x is given by

$$r(x) = r_0 + v_r(x - x_0)/v_x \qquad (2)$$

where v_x and v_r are the longitudinal and radial velocities of the plume.

We infer from experimental entrainments observed in chemical and nuclear explosive phenomena (*28*) that the high velocity jet plume will efficiently entrain rocks on a planetary surface. A similar suggestion was made by Swift and Clark (*29*).

The high velocity plume of density ρ_g when impinging upon a surface rock fragment will crush it unless the plume density is sufficiently low such that the stagnation pressure is less than the one-dimensional, compressional strength, σ_c; an upper bound is given by

$$\sigma_c = \rho_g v_x^2/2 \qquad (3)$$

Given the density and size of the plume as a function of position, an important issue is: What is the maximum size rock that can be accelerated in excess of the Martian escape velocity (5.03 km/sec)? The maximum equivalent fragment radius, r_p, that can be accelerated to velocities on the order of the plume velocity is related to the vapor plume radius as a function of position by

$$r_p = 3\rho_g x/2\rho_p \qquad (4)$$

where r_p and ρ_p are the fragment maximum radius and density. Equation 4 is derived from equating the mass of the fragment to the mass of gas required to accelerate it to escape velocity (*30*).

Equations 1 through 4 were solved to determine the maximum radius fragment that could be accelerated, without fracturing, by the jet plume as a function of impacting body radius (Fig. 3). For impactors having radii in the range of 10^{-1} to 10^0 km (which will result in craters with radii of 10^0 and 10^1 km), silicate surface fragments initially downstream of the ejecta jet having radii of at least 10 cm can be accelerated by gas entrainment to the Martian escape velocity. The mechanical and thermal regimes of

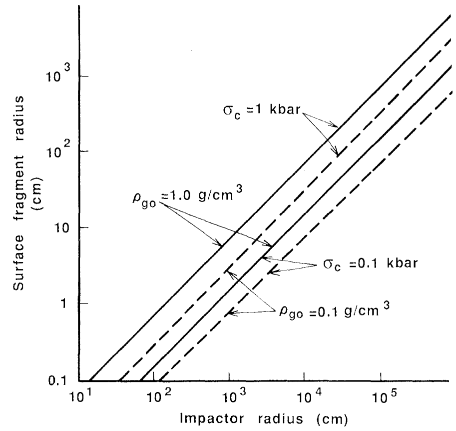

Fig. 3. Surface fragment radius accelerated to 5 km/sec by gas flow in ejecta plume, as a function of impactor radius. Lines shown for surface fragments that will survive acceleration with crushing strengths of σ_c = 1 and 0.1 kbar in flows with initial plume densities (ρ_{g0}) of 0.1 and 1 g/cm^3 for vaporized planetary and projectile material. Values of v_x = 12 km/sec, v_r = 3.3 km/sec, and x_0/r_0 = 5.0 for a 7.5-km/sec impact are assumed.

silicate fragments entrained in vapor jets require study.

The gas entrainment mechanism, even in the present two-dimensional approximation, is only slightly enhanced because of the likely higher level of CO_2 and H_2O in readily volatilized forms in the Martian regolith (*5*). Other selective mechanisms must operate to explain any preponderance of Mars samples brought to the earth in the form of SNC meteorites in preference to samples from the more refractory lunar surface (*12*).

Oblique impact induced jet plume entrainment appears to be the only mechanism that provides the physical mechanism required to explain the acceleration to high speed of lightly shocked planetary samples such as SNC meteorites.

REFERENCES AND NOTES

1. J. F. Kerridge and T. E. Bunch, in *Asteroids*, T. Gehrels, Ed. (Univ. of Arizona Press, Tucson, 1979), pp. 745–764.
2. J. T. Wasson, *Meteorites* (Springer-Verlag, New York, 1974).
3. H. Y. McSween, Jr., *Geology* **12**, 3 (1984).
4. ______, *Rev. Geophys.* **23**, 391 (1985).
5. J. T. Wasson and G. W. Wetherill, in *Asteroids*, T. Gehrels, Ed. (Univ. of Arizona Press, Tucson, 1979), pp. 926–974.
6. Except the "lunar meteorites," ALHA 81005 and Yamato 791193 appear to be samples of the lunar highlands [A. Bischoff and D. Stöffler, *Lunar Planet. Sci.* **16**, 63 (1985)].
7. J. C. Laul, M. R. Smith, R. A. Schmitt, *Geophys. Res. Lett.* **10**, 825 (1983).
8. T. K. Mayeda and R. N. Clayton, *ibid.*, p. 799.
9. ALHA 77005, a shergottite, contains xenocrysts similar to assemblages in terrestrial basalts.
10. C. A. Wood and L. D. Ashwal, *Proc. Lunar Planet. Sci.* **12B**, 1359 (1981); H. Y. McSween and E. Jarosewich, *Geophys. Cosmochim. Acta* **47**, 1501 (1983).
11. R. H. Becker and R. O. Pepin, *Eos* **64**, 253 (1983); D. D. Bogard and P. Johnson, *Science* **221**, 651 (1983).
12. G. W. Wetherill, *Meteorites* **19**, 1 (1984).

13. H. J. Melosh, *Icarus* **59**, 234 (1984); *Lunar Planet. Sci.* **16**, 548 (1985).
14. V. Ott and F. Begemann, *Nature (London)* **317**, 509 (1985); R. O. Pepin, *The Evolution of the Martian Atmosphere* (Lunar and Planetary Institute, Houston, 1985), pp. 20–21.
15. J. D. O'Keefe and T. J. Ahrens, in *Proceedings of the Eighth Lunar Science Conference* (Pergamon, New York, 1977), p. 3357; *Science* **198**, 1249 (1977).
16. C. Polanskey and T. J. Ahrens, *Lunar Planet. Sci.* **16**, 671 (1985).
17. D. E. Rehfuss, *J. Geophys. Res.* **32**, 6303 (1972).
18. A. V. Singer, *Lunar Planet. Sci.* **14**, 704 (1983).
19. L. E. Nyquist, in *Proceedings of the 13th Lunar and Planetary Science Conference* (Pergamon, New York, 1982), p. A 785.
20. A. M. Vickery, *Lunar Planet. Sci.* **16**, 877 (1985).
21. P. N. Schultz and D. E. Gault, *ibid.*, p. 740.
22. H. A. Zook *et al.*, *ibid.* **15**, 965 (1984); D. E. Gault and J. A. Wedekind, in *Proceedings of the Ninth Lunar and Planetary Science Conference* (Pergamon, New York, 1978), pp. 3843–3875.
23. S. L. Thompson, SAND 77-1339, Sandia National Labs, Albuquerque, NM (1979).
24. T. J. Ahrens and J. D. O'Keefe, *Impact and Explosion Cratering*, D. J. Roddy, R. O. Pepin, R. B. Merrill, Eds. (Pergamon, New York, 1977), pp. 639–656.
25. G. Neukum and D. U. Wise, *Science* **194**, 1381 (1976).
26. D. E. Gault, *Moon* **6**, 32 (1973).
27. G. R. Cowan and A. H. Holtzmann, *J. Appl. Phys.* **34**, 928 (1963); H. El-Sopky, in *Explosive Welding, Forming, and Compaction*, T. Z. Blazynski, Ed. (Applied Science Englewood, NJ, 1983), pp. 189–217; S. W. Kieffer, in *Impact and Explosion Cratering*, D. J. Roddy, R. O. Pepin, R. B. Merrill, Eds. (Pergamon, New York, 1977), pp. 251–770).
28. J. E. Schouten, *Nuclear Geoplosics Sourcebook* (Report DNA6501H-4-2, Defense Nuclear Agency, Washington, DC, 1979), vol. 4, part 2; H. Mirels, "Blowing model for turbulence boundary-layer dust ingestion" (SD-TR-85-97, Aerospace Corp., El Segundo, CA 1986).
29. H. F. Swift and B. C. Clark, *Lunar Planet. Sci.* **14**, 765 (1983).
30. A. Henderson-Sellers, A. Benlow, A. J. Meadows, *Q. J. R. Astron. Soc.* **21**, 74 (1980).
31. Research supported under NASA grant NSG 7129. We appreciate the assistance of M. Lainhart with the calculations. We are grateful for the helpful comments proffered by G. Wetherill, D. Stevenson, D. Anderson, J. Melosh, B. C. Clark, D. E. Gault, and M. Kovari. Contribution 4137, Division of Geological and Planetary Sciences, California Institute of Technology, Pasadena, CA 91125.

14 March 1986; accepted 11 August 1986

Structure-Activity Studies of Interleukin-2

F. E. COHEN,* P. A. KOSEN, I. D. KUNTZ, L. B. EPSTEIN, T. L. CIARDELLI, K. A. SMITH

The critical role of interleukin-2 (IL-2) in immune response heightens the need to know its structure in order to understand its activity. New computer-assisted predictive methods for the assignment of secondary structure together with a method to predict the tertiary structure of a protein from data on its primary sequence and secondary structure were applied to IL-2. This method generated four topological families of structures, of which the most plausible is a right-handed fourfold α-helical bundle. Members of this family were shown to be compatible with existing structural data on disulfide bridges and monoclonal antibody binding for IL-2. Experimental estimates of secondary structure from circular dichroism and site-directed mutagenesis data support the model. A region likely to be important in IL-2 binding to its receptor was identified as residues Leu^{36}, Met^{38}, Leu^{40}, Phe^{42}, Phe^{44}, and Met^{46}.

THE IMMUNE SYSTEM IS A COMPLEX network of effector, helper, and suppressor cells that communicate and act through a myriad of macromolecules. This system is charged with surveillance and defense of the organism against intrinsic (oncologic) or extrinsic (microbiologic) insult. The T lymphocyte is an important component of host defenses. Elucidating the roles of T cells has been facilitated by the discovery of T-cell growth factors such as interleukin-2 (IL-2) (*1*). Interest in IL-2 has increased recently owing to reports of a possible role for this lymphokine in the treatment of solid tumors (*2*). Evidence already exists for a defect in IL-2 production by T lymphocytes of patients suffering from acquired immunodeficiency syndrome (*3*) and for a partial restoration of T-cell function by the addition of exogenous IL-2 in vitro (*4*).

Computer-assisted molecular modeling can be applied to macromolecules such as proteins. Methods for the prediction of secondary structure based on primary sequence have been developed by several investigators [for example, (*5*) and references therein]. Complementary methods for examining sequence-related hydropathy (*6*) allow one to predict interior and exterior regions of proteins as well as to suggest cytoplasmic, transmembrane, and potential binding sites for cell surface receptors (*7*). These methods are evolving rapidly as databases are strengthened with increased x-ray crystallographic data and the availability of recombinant DNA-derived protein sequences.

The primary structure of human and mouse IL-2 are available from complementary DNA (cDNA) sequences (*8*). A disulfide bridge links Cys^{58} to Cys^{105} (*9*). Secondary structure was assigned to the human sequence by use of the combinatorial pattern matching scheme of Cohen *et al.* (*5*). The four regions of α-helical structure recognized are listed in the legend to Fig. 1b. This assignment satisfies the sequential spacing of turns commonly observed in α-helical proteins, while simultaneously creating hydrophobic patches that facilitate helix-helix packing (see legend to Fig. 1b) (*10*). When the human and mouse sequences are compared, several features support our secondary structure assignment. A region containing 12 consecutive glutamine residues occurs sequentially adjacent to the amino terminus of mouse IL-2 helix A. Although it is difficult to appreciate the structural significance of the polyglutamine region, it is unlikely that this insertion is helical, and it cannot be a major functional feature. Further, substitutions occur more frequently in regions assigned as nonhelical (45% to 54%). Mutations that occur in regions assigned as helical are of a very conservative nature (for example, Ile^{24} → Leu^{24} and Ile^{28} → Met^{28} in the type III patch centered on residue 24).

Structural correlates for exon boundary locations have been proposed (*11*), including functional domains and small secondary structure assemblies. Frequently, exon boundaries occur in loop regions of proteins. This is true of the IL-2 exons 1–29, 30–49, 50–98, and 99–132 (*12*), with residues 30, 50, and 99 occurring at the boundaries of the predicted secondary structure.

Cohen *et al.* (*10*) developed a scheme for predicting the three-dimensional structure of α-helical proteins from the secondary structure. They used a combinatorial approach which generated millions of possible structures that satisfied the principles of pairwise helical packing. Tertiary structure restrictions were imposed to sort out unrealistic structures. Of 3×10^7 structures that were generated for myoglobin, only two satisfied the tertiary constraints (*10*). These two structures were similar and resembled

F. E. Cohen, Department of Pharmaceutical Chemistry, School of Pharmacy, and Department of Medicine, School of Medicine, University of California, San Francisco, CA 94143.
P. A. Kosen and I. D. Kuntz, Department of Pharmaceutical Chemistry, School of Pharmacy, University of California, San Francisco, CA 94143.
L. B. Epstein, Cancer Research Institute and Department of Pediatrics, University of California, San Francisco, CA 94143.
T. L. Ciardelli, Veterans Administration Hospital, White River Junction, VT 05001, and Department of Medicine, Dartmouth Medical School, Hanover, NH 03756.
K. A. Smith, Department of Medicine, Dartmouth Medical School, Hanover, NH 03756.

*To whom correspondence should be addressed.